Gravel Liquefaction Assessment Using the Dynamic Cone Penetration Test Based on Field Performance from the 1976 Friuli Earthquake

Kyle M. Rollins, M.ASCE[1]; Sara Amoroso[2]; Giuliano Milana[3]; Luca Minarelli[4]; Maurizio Vassallo[5]; and Giuseppe Di Giulio[6]

Abstract: The dynamic cone penetration test (DPT) developed in China has been correlated with liquefaction resistance of gravelly soils based on field performance data from the M_w7.9 Wenchuan earthquake. With a diameter of 74 mm, DPT would be less sensitive to gravel size particles than the SPT or CPT and could be a viable assessment tool depending on gravel size and percentage. In this study, liquefaction resistance is evaluated using four DPT soundings with two hammer energies and shear wave velocity (V_S) measurements in Avasinis, Italy, where gravelly sand liquefied in the 1976 Friuli, Italy, earthquake. The DPT correctly predicted liquefaction at three sites where liquefaction was observed; however, it also predicted liquefaction in a highly stratified silt and silty gravel profile where ejecta was not observed. This failure appears to be a result of the "system response" of the profile, which impeded ejecta as identified at similar stratified sites in New Zealand. V_{S1}-based triggering curves often predicted no liquefaction at sites where liquefaction was observed, suggesting that the boundary curves may need to shift to the right for gravelly soils. Standard SPT energy corrections were found to be reasonable for the DPT.
DOI: 10.1061/(ASCE)GT.1943-5606.0002252.

Author keywords: Gravel; Gravel liquefaction; Dynamic cone penetrometer (DPT); Shear wave velocity; Liquefaction system response.

Introduction

One of the most challenging problems in geotechnical engineering is characterizing gravelly soils in a reliable, cost-effective manner for routine engineering projects. Even for large projects, such as dams and power projects, characterization is still expensive and problematic. This difficulty is particularly important for cases in which liquefaction may occur. As shown in Table 1, liquefaction is known to have occurred in gravelly soils in a significant number of earthquakes. As a result, engineers and geologists are frequently called on to assess the potential for liquefaction in gravels. Therefore, innovative methods for characterizing and assessing liquefaction hazards in gravels are certainly an important objective in geotechnical engineering.

In gravelly soils, the standard penetration test (SPT) and cone penetration test (CPT) are not generally useful because of interference from large-size particles. Some researchers have used gravel correction procedures or short-interval sampling (Engemoen 2007; Rhinehart et al. 2016), but these approaches are often difficult to apply. Because of the large particles, the penetration resistance increases and may reach refusal even when the soil is not particularly dense. This limitation often makes it very difficult to obtain a consistent and reliable correlation between SPT or CPT penetration resistance and basic gravelly soil properties.

To overcome this limitation, the Becker penetration test (BPT) has become the primary field test used to evaluate liquefaction resistance of gravelly soils in North American practice (Harder 1997). The Becker penetration test is performed by hammering a closed-end 168-mm-diameter casing into the ground so that the penetration resistance is much less affected by particle size. However, this test is expensive, and uncertainties exist regarding correlations with sand behavior and corrections for rod friction, chamber pressure, etc. (Cao et al. 2013; Sy 1997). Furthermore, it is simply not available for use in most of the world. Although innovative instrumentation approaches, such as the instrumented BPT (iBPT), promise to improve the reliability of energy assessment and skin friction losses for the BPT (De Jong et al. 2017), this approach does not reduce the cost and complexity of the test procedure. Furthermore, even after energy corrections, the BPT blow count must be correlated with the SPT blow count before liquefaction can be evaluated. This indirect approach increases the uncertainty in the method.

As another alternative in gravelly soils, the penetration resistance from a dynamic cone penetration test (DPT), developed in China, has been correlated with liquefaction resistance based on field performance data from the M_w7.9 Wenchuan earthquake

[1]Professor, Dept. of Civil Environmental Engineering, Brigham Young Univ., 368 CB, Provo, UT 84602 (corresponding author). ORCID: https://orcid.org/0000-0002-8977-6619. Email: rollinsk@byu.edu

[2]Assistant Professor, Dept. of Engineering and Geology, Univ. of Chieti-Pescara, Viale Pindaro, 42, 65129 Pescara, Italy; Researcher, Roma 1 Section, Istituto Nazionale di Geofisica e Vulcanologia, Viale Crispi, 43, 67100 L'Aquila, Italy. ORCID: https://orcid.org/0000-0001-5835-079X. Email: sara.amoroso@unich.it

[3]Technologist, Roma 1 Section, Istituto Nazionale di Geofisica e Vulcanologia, Via di Vigna Murata, 605, 00143, Rome, Italy. Email: giuliano.milana@ingv.it

[4]Researcher, Roma 1 Section, Istituto Nazionale di Geofisica e Vulcanologia, Viale Crispi, 43, 67100 L'Aquila, Italy. ORCID: https://orcid.org/0000-0003-3602-9975. Email: luca.minarelli@ingv.it

[5]Researcher, Roma 1 Section, Istituto Nazionale di Geofisica e Vulcanologia, Viale Crispi, 43, 67100 L'Aquila, Italy. Email: Maurizio.vassallo@ingv.it

[6]Researcher, Roma 1 Section, Istituto Nazionale di Geofisica e Vulcanologia, Viale Crispi, 43, 67100 L'Aquila, Italy. Email: giuseppe.digiulio@ingv.it

Note. This manuscript was submitted on June 22, 2018; approved on December 6, 2019; published online on March 19, 2020. Discussion period open until August 19, 2020; separate discussions must be submitted for individual papers. This paper is part of the ***Journal of Geotechnical and Geoenvironmental Engineering***, © ASCE, ISSN 1090-0241.

Table 1. Case histories involving liquefaction of gravelly soil

Earthquake	Year	M_w	Reference
Mino-Owari, Japan	1891	7.9	Tokimatsu and Yoshimi (1983)
Fukui, Japan	1948	7.3	Ishihara (1985)
Alaska	1964	9.2	Coulter and Migliaccio (1966)
Haicheng, China	1975	7.3	Wang (1984)
Tangshan, China	1976	7.8	Wang (1984)
Friuli, Italy	1976	6.4	Sirovich (1996a, b)
Miyagiken-Oki, Japan	1978	7.4	Tokimatsu and Yoshimi (1983)
Borah Peak, Idaho	1985	6.9	Youd et al. (1985), Andrus (1994)
Armenia	1988	6.8	Yegian et al. (1994)
Roermond, Netherlands	1992	5.8	Maurenbrecher et al. (1995)
Hokkaido, Japan	1993	7.8	Kokusho et al. (1995)
Kobe, Japan	1995	7.2	Kokusho and Yoshida (1997)
Chi-Chi, Taiwan	1999	7.8	Lin and Chang (2002)
Wenchuan, China	2008	7.9	Cao et al (2013)
Cephalonia, Greece	2012	6.1	Nikolaou et al. (2014)
Pedernales, Ecuador	2016	7.8	Lopez et al. (2018)

(Cao et al. 2013). The DPT consists of a 74-mm-diameter cone tip continuously driven by a 120-kg hammer with a free-fall height of 100 cm, using a 60-mm drill rod to reduce friction. The DPT blow count, N_{120}, represents the number of hammer blows to drive the penetrometer 30 cm with a 120-kg hammer. Blow counts are typically reported every 10 cm but are multiplied by 3 to get the equivalent N_{120}.

Over the past 60 years, Chinese engineers have found that the DPT is effective in penetrating coarse or cobbly gravels and provides penetration data useful for liquefaction assessment (Cao et al. 2013). This test could provide an important new procedure for characterization of gravels and fill a gap in present geotechnical practice between CPT/SPT and BPT testing, but additional field performance data is necessary. At 74 mm, the DPT diameter is 50% larger than the SPT and 110% larger than a standard 10-cm^2 CPT; however, it is still 55% smaller than the BPT. Clearly, the BPT provides the best diameter-to-particle-size ratio of all the tests, but the DPT would be superior to the SPT or CPT and could be a reasonable solution in many cases depending on gravel size and percentage. The effect of both gravel size and percentage on the DPT penetration resistance must be studied more comprehensively in the future. Remarkably, Cao et al. (2013) reported that the DPT penetration resistance was able to differentiate liquefaction from no liquefaction at some sites with maximum particle sizes of 70 mm, despite the low diameter-to-particle-size ratio.

As with the BPT, side friction effects need to be considered with the DPT. The BPT has a constant diameter for its entire length, whereas the drill rods for the DPT are 60 mm in diameter relative to the 74-mm diameter of the cone. This difference in diameter is likely to produce a significant reduction in side friction during penetration. Cao et al. (2013) stated that Chinese experience with the DPT "indicates that rod friction is negligible for depths less than 20 m for all soils except soft clays." Fortunately, as noted by Cubrinovski et al. (2017), "in the updated database of liquefaction manifestation case histories of Boulanger and Idriss (2014), out of over 250 CPT-based case histories there is only one case in which the depth of the critical layer (liquefaction) was greater than 10 m." Nevertheless, we believe that the rod friction issue deserves further investigation, because liquefaction evaluations are still necessary at greater depths. In addition, it would be desirable to independently confirm the Chinese experience.

The shear wave velocity (V_S) has also been used as a means to evaluate the liquefaction resistance of sands and gravel liquefaction. However, a number of studies have indicated that the boundary for liquefaction triggering may be higher for gravels than for sands (Chang et al. 2016; Cao et al. 2013). For example, Stokoe et al. (2015) and Menq (2003) have shown that V_S is higher in gravels than in sands at the same relative density. Therefore, additional shear wave velocity data would be desirable at field sites where gravels have or have not liquefied. The objective of this paper is to provide additional DPT and V_S data for gravel liquefaction case histories from the 1976 Friuli, Italy earthquake. These sites experienced liquefaction during the main shock (M_w6.4) and during two subsequent aftershocks (M_w6 and M_w5.3). Therefore, these case histories can be particularly instructive in defining liquefaction-triggering curves.

Geologic Setting and Liquefaction Case Histories

The sediments in Avasinis are late Quaternary intramontane deposits of alluvial and fluvioglacial origin (Fontana et al. 2008; Zanferrari et al. 2013). These sediments were deposited by two mountain creeks (Rio Canale and Torrente Leale) that produced a composite alluvial fan. The composite fan shows a clear lateral gradient in grain size, with gravelly sediments near the apex of the fan and sandy sediments lower on the fan. According to Sirovich (1996b), the sands and gravels in the upper 10 m of the profile are between 100 and 1,000 years old.

The sediment type distribution is shown in Fig. 1 based on a critical reinterpretation of previous data (Sirovich 1996b; Serravalli 2016). The stream running at the base of the alluvial fan (Torrente Leale) has reworked the lowermost portion of the fan. The stream maintains the water table relatively high in the lower portion of the highly permeable sediments of the fan, a factor playing a crucial role in the potential for liquefaction. Fig. 1 shows the ground surface topography and liquefaction features in the vicinity of Avasinis, together with the locations of the four gravel test sites investigated.

According to Sirovich (1996b), in the 1976 Friuli earthquake, sand and gravel ejecta were observed in numerous blows and fissures in the northwestern side of the fan, whereas sand ejecta was primarily observed in hundreds of sand blows in the southeastern side of the fan, as shown in Fig. 1. DPT soundings 1, 2, and 3 were located in areas where sand and gravel ejecta were observed, and DPT 4 was also located on the upper western side of the fan but in an area where no liquefaction features were observed. Houses and garages near Sites 1 and 2 settled as much as 60 cm and suffered severe cracking of floor slabs. The gravelly soils in the upper part of the fan are composed of angular to semiangular limestone particles within a weak structure that ranges from gravel clast-to-clast supported to matrix supported (Sirovich 1996b).

Samples for gradation testing were obtained from 100-mm-diameter core holes. Because the maximum particle size was between 25 and 40 mm, the core diameter did not likely affect the measured particle-size distributions. Particle-size distribution curves at the location of DPT 1 are provided in Fig. 2 (Sirovich 1996b). Although data is very limited, the gravel fraction appears to increase with depth, and fines contents are typically around 10% to 15%. Based on the Unified Soil Classification System (USCS) that defines gravel size as coarser than 4.75 mm, the gravel fraction is between 20% and 40%. However, many organizations define gravel as coarser than 2 mm, and based on that definition, the gravel content would be between 40% and 60% [AASHTO M 145 (AASHTO 1995); EN ISO 14688-1 (ISO 2018); BS 5930 (BSI 2015)]. Fig. 3 shows sieve analyses at the location of DPT 4. The gravel fraction is more consistent than at Site 1, but the fines contents range between 1% and 26%, with an average of 13%. The fines were generally nonplastic. According to the USCS,

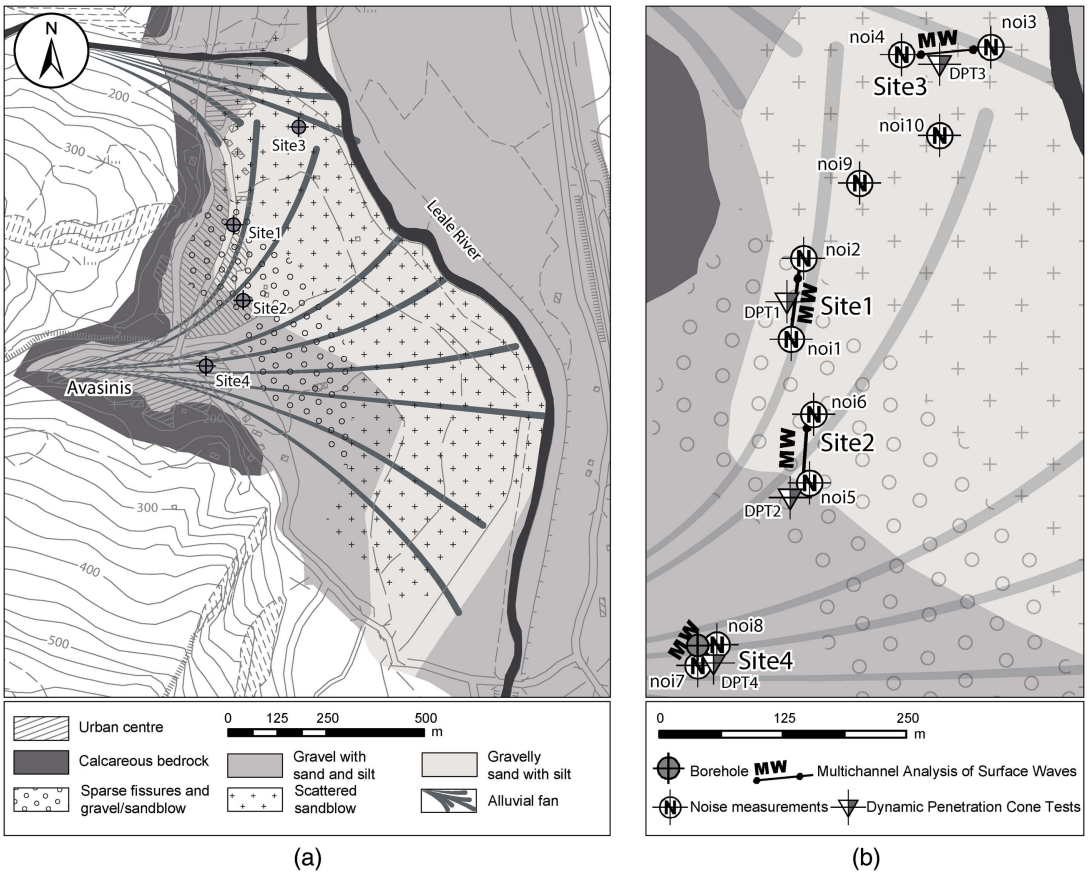

Fig. 1. Site map showing: (a) locations of test sites with respect to topography and location of sand ejecta and sand/gravel ejecta; and (b) locations of geotechnical and geophysical investigations. (Data from Sirovich 1996b; Serravalli 2016.)

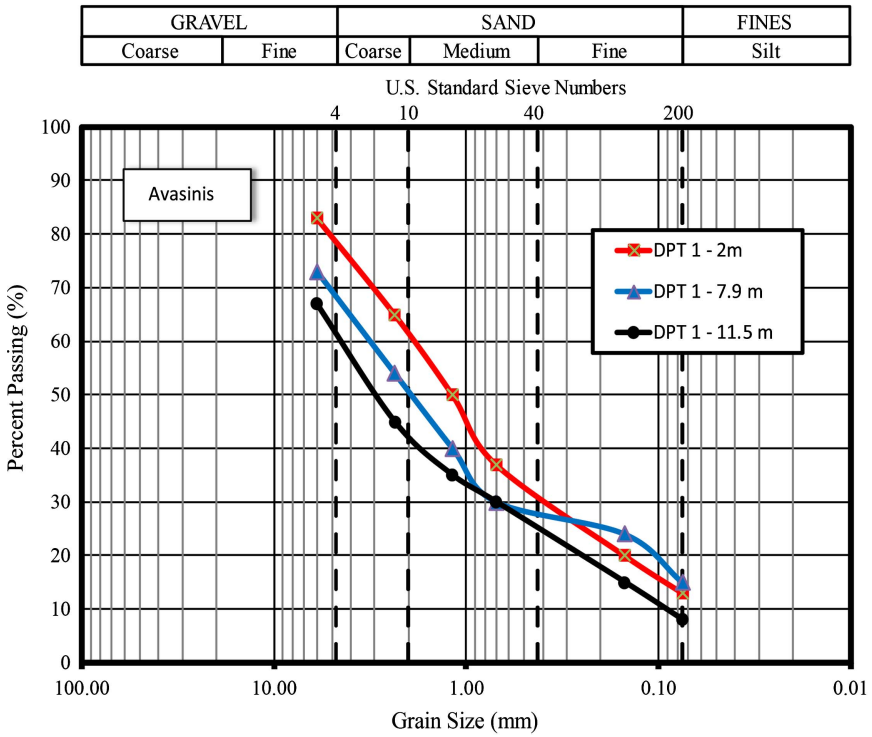

Fig. 2. Particle size distribution curves for selected test specimens at DPT 1 site. (Data from Sirovich 1996b.)

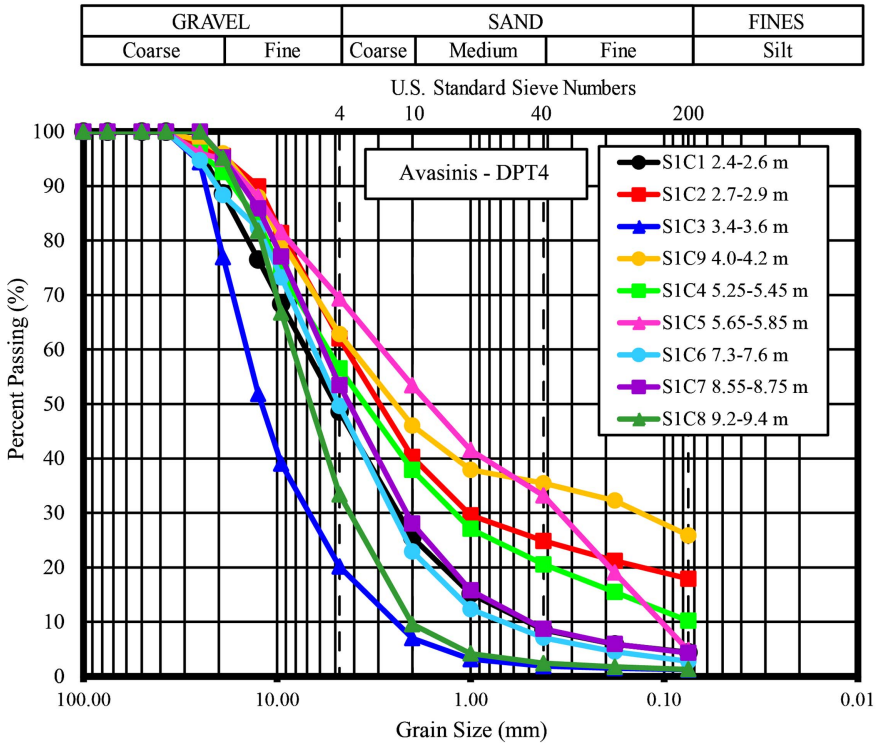

Fig. 3. Particle size distribution curves for selected test specimens at DPT 4 site.

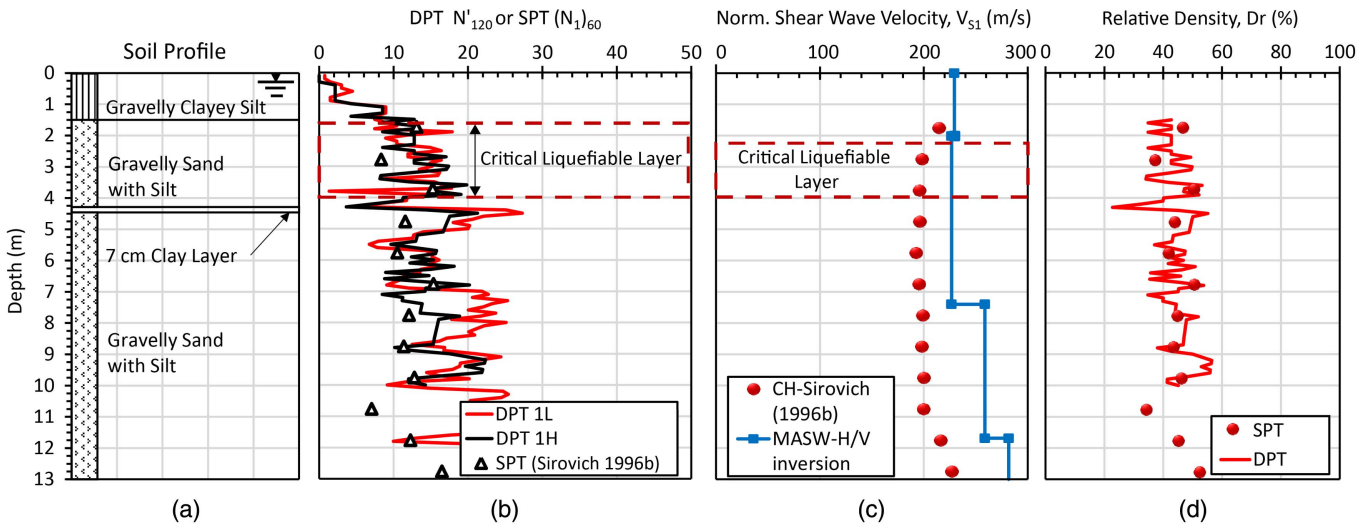

Fig. 4. DPT 1: (a) soil profile; (b) DPT N'_{120} versus depth for heavy (H) 120-kg and light (L) 63.5-kg hammer in comparison with SPT $(N_1)_{60}$ versus depth Sirovich (1996a); (c) normalized shear wave velocity (V_{S1}) profiles from cross-hole and joint inversion of H/V and MASW dispersion curve; and (d) relative density from SPT and DPT correlations.

the gravel fraction is typically around 30% to 50%, whereas it is between 50% and 80% when the gravel size is defined as greater than 2 mm.

DPT Soundings

As part of this study, DPT soundings were performed at three sites where gravelly sand ejecta was observed (Sites 1, 2, and 3) and one site where no liquefaction features were observed (Site 4). The soil profile at Site 1, shown in Fig. 4(a), is based on an SPT borehole previously drilled by Sirovich (1996a) on a roadway about 20 m west of Site 1. The soil profile was generally described as gravelly alluvium up to a depth of 30 m; however, the DPT 1 site has a weak surface layer about 1.5 m thick consisting of gravelly clayey silt. This surface layer appears to have been excavated and replaced with a denser gravel fill beneath the roadway. The N values obtained by Sirovich (1996a) from SPT tests with a safety hammer have been corrected to $(N_1)_{60}$ values using procedures outlined by Youd et al. (2001) based on a measured SPT hammer energy of 42% reported by Sirovich (1996a). Although the energy ratio is relatively low, it is well within the range of measured values for safety hammers reported by Kovacs et al. (1983), and Sirovich (1996a) could find

J. Geotech. Geoenviron. Eng., 2020, 146(6): 04020038

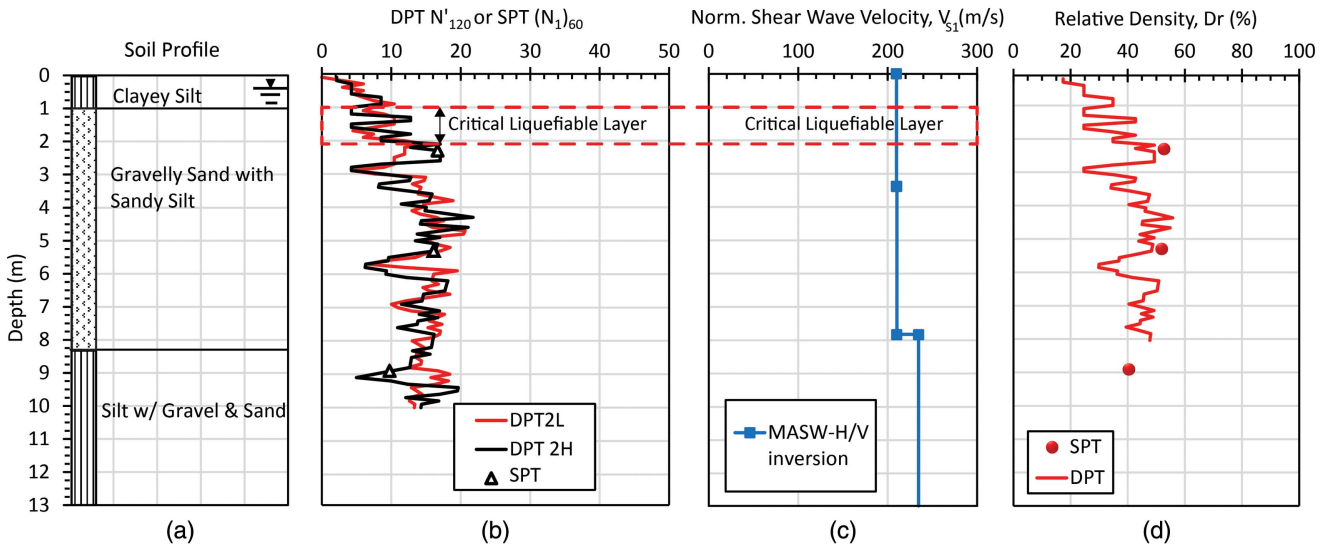

Fig. 5. DPT 2: (a) soil profile; (b) DPT N'_{120} versus depth for heavy (H) 120-kg and light (L) 63.5-kg hammer in comparison with SPT $(N_1)_{60}$ versus depth; (c) normalized (Norm.) shear wave velocity (V_{S1}) profiles from joint inversion of H/V and MASW dispersion curve; and (d) relative density from SPT and DPT correlations.

no problems with the testing procedure performed in accordance with ISSMFE (1988) standards. The resulting $(N_1)_{60}$ values are plotted in Fig. 4(b). The $(N_1)_{60}$ values typically range from 12 to 16 within the upper 12 m of the profile. There is no obvious influence of gravel on the SPT results, but this is not surprising considering that the profile is relatively homogeneous and does not contain interbedded layers of gravel and sand.

The DPT soundings were performed with a drill rig able to use two different hammer energies. At each site, one DPT sounding was advanced using a free-fall SPT donut hammer with a weight of 63.5 kg (140 lb) dropped from a height of 0.76 m (30 in.). A second sounding was then performed about 1.5 m away using a 120-kg (265-lb) free-fall donut hammer with a drop height of 1.0 m (39 in.). This spacing was a compromise between having the holes close enough that they would encounter similar soil profiles but far enough apart that the subsequent hole would not be affected by the presence of the previous hole. Hammer energy measurements were made using an instrumented rod section and a Pile Driving Analyzer (PDA) device from Pile Dynamics, Inc. (Cleveland, Ohio). These energy measurements indicate that the SPT and 120-kg hammers delivered averages of 65% and 75% of their theoretical free-fall energies, respectively, with standard deviation values of 5.6% and 5.9%. Based on 1,200 hammer energy measurements, Cao et al. (2012) found that the Chinese DPT provided an average of 89% of the theoretical free-fall energy. Because the energy delivered by a given hammer (E_{Hammer}) may be less than the energy typically supplied by a Chinese DPT hammer ($E_{\text{Chinese DPT}}$), it may be necessary to correct the measured blow count downward. In this study, the correction was made using the simple linear reduction suggested by Seed et al. (1985) for SPT testing:

$$N_{120} = N_{\text{Hammer}}(E_{\text{Hammer}}/E_{\text{Chinese DPT}}) \tag{1}$$

where N_{Hammer} = number of blows per 0.3 m of penetration obtained with a hammer delivering an energy of E_{Hammer}.

The ratio of hammer energy actually delivered divided by the energy delivered by the Chinese DPT hammer was 0.84 for the 120-kg hammer and 0.29 for the 63.6-kg hammer. In addition, Cao et al. (2013) recommended an overburden correction factor, C_n, to obtain the normalized N'_{120} value using the equation

$$N'_{120} = N_{120}C_n \tag{2}$$

where

$$C_n = (100/\sigma'_o)^{0.5} \leq 1.7 \tag{3}$$

as originally proposed by Liao and Whitman (1986); and σ'_o = initial vertical effective stress in kN/m^2. In this study, a limiting value of 1.7 was added to be consistent with the C_n used to correct penetration resistance from other in situ tests (Youd et al. 2001).

Plots of the energy-corrected DPT N'_{120}-versus-depth profiles for the 63.5- and 120-kg hammers are provided in Figs. 4(b), 5(b), 6(b), and 7(b) for DPT soundings 1, 2, 3, and 4, respectively. A comparison of these profiles indicates that the agreement obtained with the simple energy correction factor in Eq. (2) is quite good. In addition to variations due to differences in hammer energy, it should be recognized that differences in N'_{120} would also be expected between soundings with the same hammer energy because of small differences in site elevation and soil stratigraphy, even though the DPT soundings are relatively close together. It should also be noted that about 1.6 m of fill were placed at Site 4 subsequent to the 1976 earthquake [Fig. 7(a)].

A comparison of the energy-corrected N'_{120} obtained from the lighter 63.5-kg hammer typically used with SPT testing and that obtained with the heavier 120-kg hammer used with the Chinese DPT at each depth is provided in Fig. 8(a) for all the DPT tests at Avasinis. The best-fit regression line for all 430 data pairs falls on the one-to-one line for perfect agreement, indicating that the average DPT N'_{120} values are comparable after energy correction; however, there is scatter about the best-fit line, and the correlation coefficient is only 63%. Of course, scatter would be expected even if the same hammer energy was used at two adjacent soundings, as a result of local variations in stratigraphy and gradation. To minimize the effects of these local variations, plots of cumulative energy-corrected N'_{120} values were produced for each pair of soundings as shown in Fig. 8(b) for Site 2. The difference between the two curves in Fig. 8(b) is less than 5%, and differences for all sites were less than 10%. This result indicates that the typical SPT-based energy correction (Seed et al. 1985) is reasonable for the DPT.

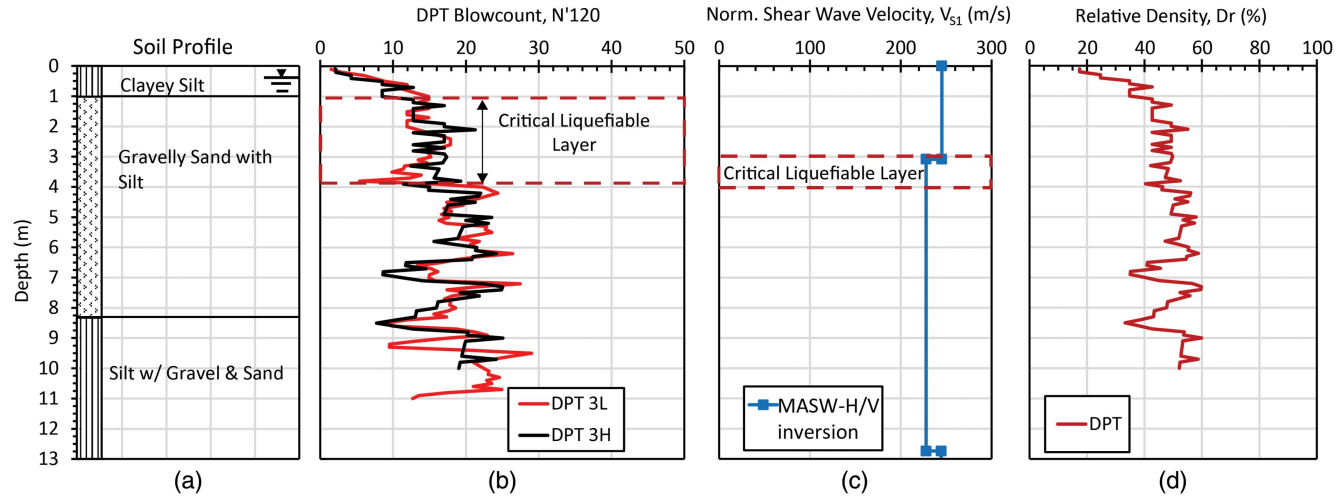

Fig. 6. DPT 3: (a) soil profile; (b) DPT N'_{120} versus depth for heavy (H) 120-kg and light (L) 63.5-kg hammer; (c) normalized (Norm.) shear wave velocity (V_{S1}) profiles from joint inversion of H/V and MASW dispersion curve; and (d) relative density from DPT correlations.

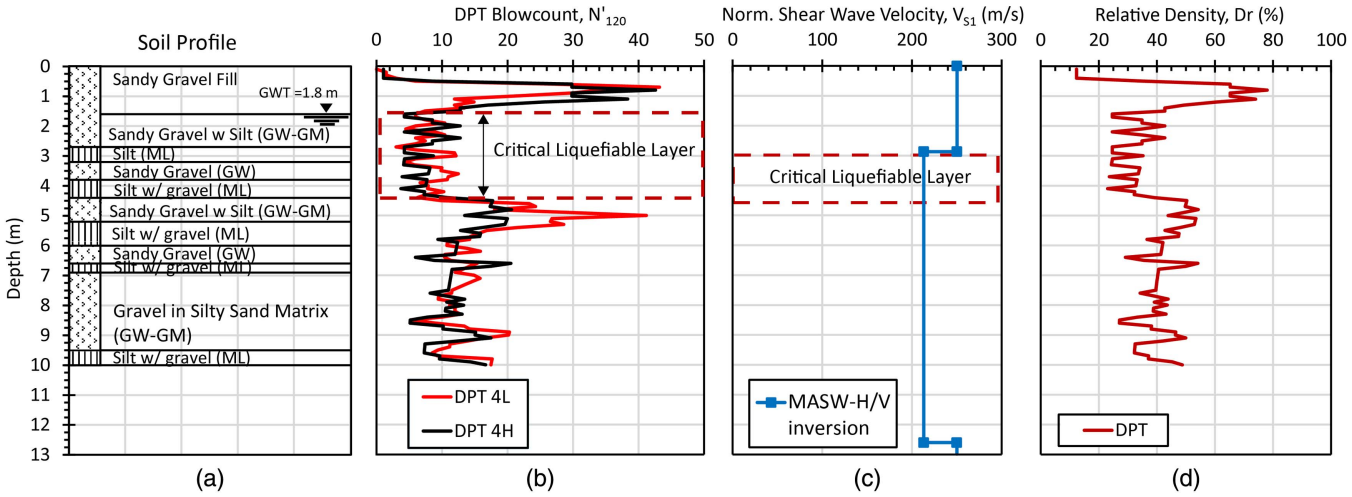

Fig. 7. DPT 4: (a) soil profile; (b) DPT N'_{120} versus depth for heavy (H) 120-kg and light (L) 63.5-kg hammer; (c) normalized (Norm.) shear wave velocity (V_{S1}) profiles from joint inversion of H/V and MASW dispersion curve; and (d) relative density from DPT correlations.

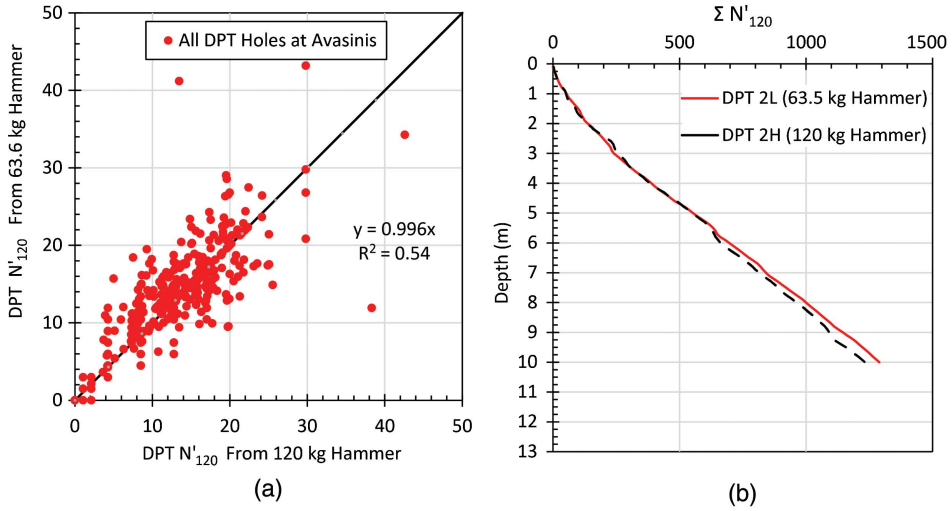

Fig. 8. Comparison of (a) energy-corrected DPT N'_{120} values from 63.5- and 120-kg hammers at each depth; and (b) cumulative energy-corrected DPT N'_{120} for 63.5- and 120-kg hammers at Site 2.

In addition to the DPT N'_{120} values, conventional SPT tests were previously performed by Sirovich (1996a) near the locations for DPT 1 and DPT 2, and $(N_1)_{60}$ values are plotted in Figs. 4(b) and 5(b). Although the SPT $(N_1)_{60}$ values appear to exhibit trends similar to the DPT N'_{120} values, no useful correlation could be developed with the very small data set (15 SPT N_{60} values). Nevertheless, investigations by Talbot (2018) based on tests at gravel sites in Idaho indicated that the SPT N_{60} is 75% of the DPT N_{120}, on average. Unfortunately, the data scatter is significant, and correlation is relatively poor ($r^2 = 0.45$), considering that gravel content impacts the SPT and DPT penetration resistance in substantially different ways.

The relative density (D_r) was computed based on the SPT $(N_1)_{60}$ values near DPT 1 and 2 using the equation

$$D_r = [(N_1)_{60}/60]^{0.5} \tag{4}$$

proposed by Kulhawy and Mayne (1990), and D_r was computed for the DPT N'_{120} values at each site using the equation

$$D_r = (N'_{120}/70)^{0.5} \tag{5}$$

suggested by Chinese experience with the DPT (Chinese Design Code 2001).

Relative density profiles are also plotted in Figs. 4(d), 5(d), 6(d), and 7(d). Relative density values are typically between 40% and 50% at most sites. A comparison of the D_r from the DPT and SPT values for DPT 1 and 2 is provided in Figs. 4(d) and 5(d), and the agreement between the two approaches appears to be relatively good for this limited data set.

Shear-Wave Velocity Measurements

The normalized V_{S1} profile based on cross-hole testing near the DPT 1 site reported by Sirovich (1996a) is plotted as a function of depth in Fig. 4(c). The V_S values reported by Sirovich (1996a) were corrected for overburden pressure to obtain V_{S1} using the equation

$$V_{S1} = V_S(P_a/\sigma'_o)^{0.25} \tag{6}$$

proposed by Sykora (1987), Robertson et al. (1992), and Kayen et al. (1992) and adopted by Youd et al. (2001), where P_a = atmospheric pressure approximated by a value of 100 kPa. After correction, the V_{S1} profile is almost constant at a value of 200 m/s from the ground surface to a depth of 11 m.

As part of this study, V_S profiles were also developed using multi-channel analysis of surface waves (MASW) (Park et al. 1999) near each DPT site [Fig. 1(b)]. MASW surveys were performed using a linear array at each site composed of vertical 4.5-Hz geophones connected by three multichannel stations (Geode manufactured by Geometrics, San Jose, California). Both active and passive data were collected and processed with a frequency-wavenumber (f-k) analysis (e.g., Tokimatsu 1997) through the Geopsy package (http://www.geopsy.org). The aim of the MASW measurements is to derive the apparent phase-velocity dispersion curve; an inversion of the experimental dispersion curve provides the local V_S profile (Foti et al. 2017).

Active measurements were made using a 5-kg sledgehammer striking an iron plate as the seismic source. The source was aligned to the geophones and was located at five different offsets for each linear array. For a single offset, a stack of three measurements was acquired to increase the signal-to-noise ratio. Passive measurements were performed using ambient seismic noise. Active measurements were sampled at 8,000 Hz for a duration of 2 s for each seismic trace, whereas passive measurements were sampled at 500 Hz for a duration from 5 to 20 min depending on the site.

At Sites 1, 2, and 3, a total of 72 geophones were equally spaced at 1-m intervals along the acquisition line. The shots were situated −2 and −8 m from the first geophone, +2 and +8 m from the last geophone, and at the center of the linear array. Because of space constraints at Site 4, active measurements were made using 48 vertical geophones with 0.5-m spacing [Fig. 1(b)]. In this case, the offset source was −1 and −3 m from the first geophone, +1 and +3 m from the last geophone, and at the middle. At Site 4, the passive measurements were performed with 72 geophones in a two-dimensional geometry in the shape of a cross.

As an example of f-k analysis, Fig. S1 shows the surface-wave dispersion curves derived from active data. The experimental dispersion curves are clear, and the results at different offset are consistent; however, in some cases, the f-k analysis shows indications of higher modes (although higher modes were not considered during the inversion). In addition to the MASW measurements, 10 single-station seismic noise measurements [Fig. 1(b)] were acquired to compute the horizontal-to-vertical Fourier amplitude spectral ratios (H/V curves). The H/V method (Nakamura 1989; Fäh et al. 2003; Piña-Flores et al. 2016, among many other papers) is widely used in seismological and microzoning studies to investigate site effects. The resonance frequency (f_0) derived from the peak of the H/V curve is a proxy of the seismic impedance contrast between the uppermost soft layer and stiff bedrock (e.g., Bonnefoy-Claudet et al. 2006). For H/V noise measurements, the recording equipment was composed of three-component velocimeters (Lennartz 5s; Remscheid, Germany) connected to a 24-bit digitizer (REF TEK 130; Plano, Texas). The duration of recording ranged from 1 to 2 h depending on the site. For each MASW site, two noise measurements were carried out near the extreme limit (i.e., in proximity to the first and last geophones) of the linear array [Fig. 1(b)]. Two additional noise measurements (noi9 and noi10) were performed between Sites 3 and 4.

Figs. 9 and S2 show that, proceeding from north to south within the target area, H/V curves are characterized by a higher frequency value f_0, and the amplitude level of the H/V peak also increases. Indeed, the f_0 value is lower than 2 Hz for Site 3 but increases for Sites 1 and 2. For Site 4, the H/V peak is very narrow, and the f_0 is about 3 Hz (Fig. 9). The H/V curves suggest that the depth to bedrock increases from south (Site 4) to north (Site 3).

The experimental H/V ratios (up to 5 Hz) and dispersion curves were jointly inverted with a dedicated code to obtain best-fit velocity models. The selected code of inversion is based on the diffuse field assumption (Piña-Flores et al. 2016) and the theoretical connection between the elastodynamic Green's functions (imaginary part) and the H/V curve (Sánchez-Sesma et al. 2011). As model parameterization, we used 10 layers, in each of which the free parameters (compression wave velocity, shear wave velocity, thickness, Poisson ratio, and density) were allowed to vary during the inversion procedure (Table S1). No strong constraints were used for each free parameter. In this way, we performed a "pseudo-global" search of parameters in a very large range of plausible values. For simplicity of the inversion process, shear-wave velocity was considered to increase with depth (i.e., no velocity inversion was allowed in the V_S profile). The inversion of the experimental H/V and surface wave dispersion curves, obtained from MASW, was initially based on a Monte Carlo sampling followed by an interior-point or downhill-simplex inversion algorithm (García-Jerez et al. 2016). The code ultimately computed a total of 1,400 to 3,200 inverted models depending on the site. As an example, Fig. S3 displays the inverted velocity models at Site 1 obtained from the joint inversion analysis.

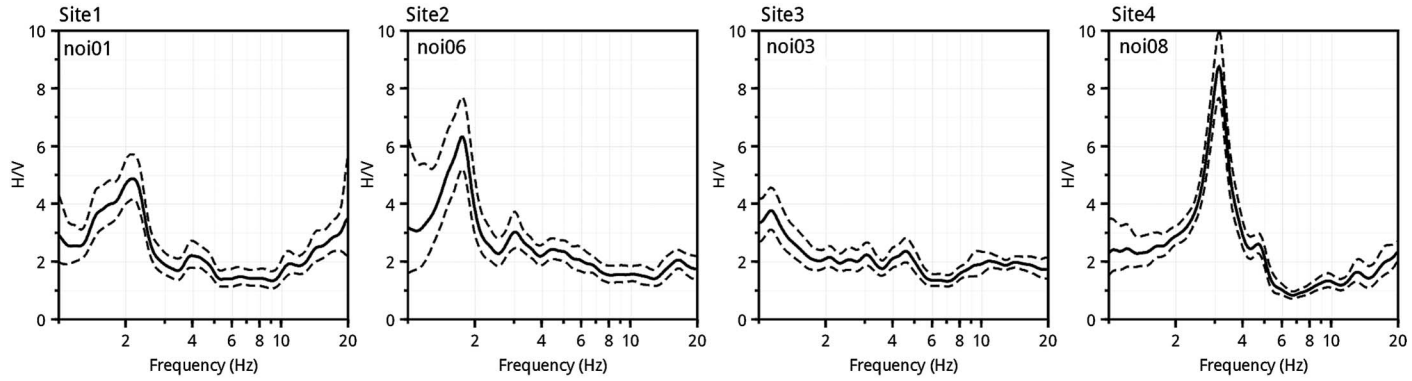

Fig. 9. H/V curves (mean ± 1 standard deviation as continuous and dashed curves, respectively). The location of noise measurements is reported in Fig. 1(b).

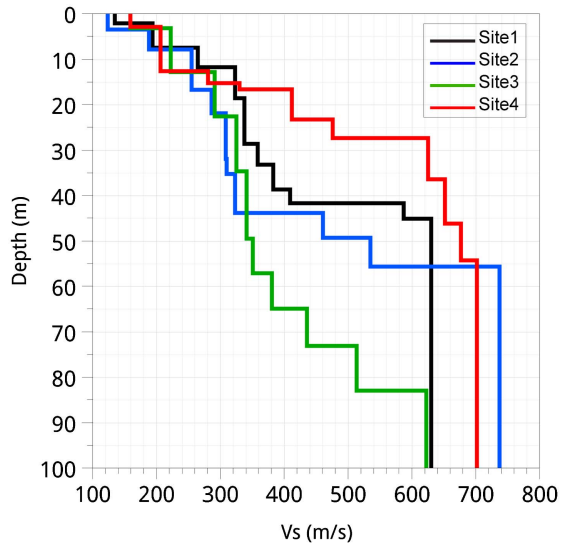

Fig. 10. Best shear-wave velocity (V_S) models derived from the joint inversion of the experimental H/V and MASW dispersion curves. The best V_S models obtained at each site are overlaid to better show velocity variation within the four sites.

The best-fitting V_S models obtained from the inversion process at the four sites are compared in Fig. 10. The V_S values of the velocity profiles range from 100 near the surface to 600–800 m/s at the bedrock interface. The bedrock depth obtained from inversion is about 80 m deep at Site 3 in the north part of the target area, whereas it is only 30 m deep at Site 4 in the south, consistent with the high-frequency peak of the H/V curve at this site (Fig. 9). In an inversion process, the starting model parameterization could influence the final results (Cox and Teague 2016). However, the adopted model parameterization (Table S1) and the inversion strategy were kept fixed during the inversion process at all four sites; thus the discrepancies among V_S profiles in Fig. 10 cannot be ascribed to the starting parameterization. Interpreted V_{S1} values after overburden correction using Eq. (6) are summarized for each site in Table 2.

Normalized shear wave velocity profiles interpreted from both cross-hole and MASW dispersion curves and H/V data inversion are provided in Figs. 4(c), 5(c), 6(c), and 7(c) for Sites 1, 2, 3, and 4, respectively, for the depth range corresponding to the DPT tests. V_{S1} values in the zone below the water table and above a depth of 13 m were typically between 210 and 240 m/s. The velocities interpreted from the joint inversion at Site 1 are somewhat higher than the cross-hole values. This discrepancy may result from the difference in location or the greater measurement lengths used in the MASW testing relative to the small measurement interval used in the cross-hole tests. However, the higher velocities may also result, in part, from aging, considering that these geophysical measurements were carried out more than 20 years after the cross-hole surveys.

Comparison with DPT-Based Liquefaction-Triggering Curves

After the 2008 M_w7.9 Wenchuan earthquake in China, 47 DPT soundings were made at 19 sites with observed liquefaction effects and 28 nearby sites without liquefaction effects. Most of those sites

Table 2. Summary of normalized shear wave velocity profiles at the four DPT sites obtained from MASW and noise measurements

DPT 1		DPT 2		DPT 3		DPT 4	
Depth (m)	V_{S1} (m/s)	Depth (m)	V_{S1} (m/s)	Depth (m)	V_{S1} (m/s)	Depth (m)	V_{S1} (m/s)
0.0–2.0	229	0.0–7.8	210	0.0–3.1	245	0.0–2.9	250
2.0–7.4	227	7.8–31.9	234	3.1–12.7	228	2.9–12.6	213
7.4–11.7	259	31.9–43.8	221	12.7–22.6	245	12.6–15.2	250
11.7–18.6	282	43.8–49.3	303	22.6–34.7	242	15.2–16.6	284
18.6–28.5	264	49.3–55.6	342	34.7–49.5	230	16.6–23.2	335
28.5–33.2	262	—	—	49.5–57.1	223	23.2–27.4	365
33.2–38.6	269	—	—	57.1–64.9	234	27.4–36.3	453
38.6–41.6	279	—	—	64.9–73.1	260	36.3–46.1	442
41.6–45.1	393	—	—	73.1–82.9	355	46.1–54.2	437

consisted of 2–4 m of clayey soils, which in turn were underlain by gravel beds up to 500 m thick. Looser upper layers within the gravel beds are the materials that liquefied during the Wenchuan earthquake. Because samples are not obtained with DPT, boreholes were drilled about 2 m away from most DPT soundings, with nearly continuous samples retrieved using core barrels. DPT soundings reached depths as great as 15 m, readily penetrating gravelly layers that liquefied as well as many layers that were too dense to liquefy.

Layers with the lowest DPT resistance in gravelly profiles were identified as the most liquefiable or critical liquefaction zones. At sites with surface effects of liquefaction, these penetration resistances were generally lower than those at nearby DPT sites without liquefaction effects. Thus, low DPT resistance became a reliable identifier of liquefiable layers (Cao et al. 2011). At the center of each layer, the cyclic stress ratio (CSR) induced by the earthquake was computed using the simplified equation

$$CSR = 0.65(a_{\max}/g)(\sigma_{vo}/\sigma'_{vo})r_d \quad (7)$$

where $a_{\max}$ = peak ground acceleration; σ_{vo} = initial vertical total vertical stress; σ'_{vo} = initial vertical effective stress; and r_d = a depth reduction factor, as defined by Youd et al. (2001).

Using DPT data, Cao et al. (2013) plotted the cyclic stress ratio causing liquefaction against DPT N'_{120} values for the M_w7.9 Wenchuan earthquake. Points where liquefaction occurred are shown as solid red dots, and sites without liquefaction are shown with open circles (Fig. 11). Cao et al. (2013) also defined curves indicating 15%, 30%, 50%, 70%, and 85% probability of liquefaction based on logistical regression. To facilitate comparison with data points from other earthquakes, in this study the Cao et al. (2013) data points and triggering curves were shifted upward using the equation

$$CSR_{M_w7.5} = CSR/MSF \quad (8)$$

where the magnitude scaling factor (MSF) is given by the equation

$$MSF = 10^{2.24}/M_w^{2.56} \quad (9)$$

proposed by Youd et al. (2001). More recent magnitude scaling factor equations have been developed, but they typically require an assessment of relative density or include SPT or CPT penetration resistance, which makes their applicability questionable or difficult for gravel sites. Efforts are now underway to expand the DPT-based gravel liquefaction case history data set (Cao et al. 2019).

The four Avasinis locations with DPT test results provide an excellent opportunity to evaluate the ability of the DPT-based liquefaction-triggering curves developed by Cao et al. (2013) to accurately predict liquefaction in gravelly soil. For the Friuli case histories, the geology, earthquake magnitude, and gravel layers are significantly different from those in the Chengdu plain of China and provide a good test of the method. In addition, gravelly soils at Site 1 are reported to have liquefied in three separate earthquake events (Sirovich 1996b), so three separate data points can be generated for this site.

At each site, the critical layer for liquefaction was selected as the layer most likely to trigger and manifest liquefaction at the ground surface (Cubrinovski et al. 2018). Typically, this was the gravelly layer with the lowest average N'_{120} below the water table and cohesive surface layer relative to the CSR curve at the site. The critical layer was typically selected over an interval of 1 m or more in an effort to provide a more representative N'_{120} value that was less affected by thin peaks or troughs (Boulanger and Idriss 2014). The critical layers for each DPT profile are indicated in Figs. 4(b) through 7(b). At Site 1, a deeper layer from 5.5 to 7 m had a similar CSR- N'_{120} value, but the thicker upper layer was selected as the critical layer because it was more likely to produce the observed liquefaction features (Green et al. 2014). Ultimately, this choice had no effect on subsequent evaluations, because the CSR-N'_{120} points were similar. The average soil properties, vertical soil stresses, and r_d values for the critical layer at each site are summarized in Table 3. Moment magnitudes for the three earthquakes for which liquefaction was reported were obtained from the Engineering Strong Motion database (Luzi et al. 2016), as shown in Table 4.

Although there were no seismographs in Avasinis during the earthquakes in Friuli, there were a number of seismographs in the vicinity that can aid in selecting an appropriate peak ground acceleration (PGA) or $a_{\max}$ for each event. Boulanger and Idriss (2014) reported that the "large majority" of sites in the CPT liquefaction case history database did not have nearby strong motion recordings and had to be estimated.

Initially, we looked at the recorded PGAs at strong motion sites on similar soil profiles (Class B) located at similar hypocentral distances from the earthquake focus for each event. We then checked these values for reasonableness using a ground motion prediction

Table 3. Summary of average soil properties and earthquake parameters in critical liquefaction layer

	Soil properties								Earthquake characteristics			
									M_w6.4	M_w6.0	M_w5.3	
									MSF = 1.5	MSF = 1.77	MSF = 2.43	
Site	Avg. depth (m)	Avg. σ_o (kPa)	Avg. σ'_o (kPa)	Avg. N'_{120} (blows per 0.3 m)	Avg. $(N_1)_{60}$ (blows per 0.3 m)	Avg. fines (%)	Avg. $(N_1)_{60,cs}$ (blows per 0.3 m)	Avg. V_{S1} (m/s)	$a_{\max}$ = 0.47 CSR/MSF	$a_{\max}$ = 0.25 CSR/MSF	$a_{\max}$ = 0.25 CSR/MSF	Depth factor r_d
1	2.5	47.5	25.9	12.3	12.3	13	14.7	200	0.36	0.16	0.12	0.98
2	1.5	28.3	16.5	7.7	17	10	18.2	210	0.33	—	—	0.99
3	3.0	57.7	31.3	15.0	—	—	—	228	0.36	—	—	0.98
4	3.0	57.7	31.3	7.2	—	—	—	213	0.36	—	—	0.98

Table 4. Summary of seismological characteristics of 1976 Friuli earthquakes in Avasinis, Italy

Earthquake data and origin time	Latitude (°)	Longitude (°)	Depth (km)	M_w	Fault type	$a_{\max}$ in Avasinis (g)
1976-05-06 20:00:12	46.262	13.300	5.7	6.4	Thrust faulting	0.46
1976-09-15 09:21:18	46.300	13.174	11.3	6.0	Thrust faulting	0.25
1977-09-16 23:48:07	46.283	13.019	10.8	5.3	Thrust faulting	0.25

equation (GMPE) developed for Italy (Bindi et al. 2011) and with USGS ShakeMaps (Worden et al. 2020). The Bindi et al. (2011) GMPE was developed using the Joyner–Boore distance (the closest distance from the site to the surface projection of the rupture fault plane), or hypocentral distance, and considers the style-of-faulting and site effects. USGS ShakeMaps incorporate a weighted-average approach for combining different types of data (e.g., recordings, intensities, ground motion prediction equations) to arrive at best estimates of peak ground motion parameters. Boulanger and Idriss (2014) used ShakeMaps to check PGA estimates for a number of sites in their liquefaction case history database with no nearby recordings.

For the M_w5.3 event, the hypocentral distance from Avasinis was 11.2 km. PGAs at strong motion recording stations FRC and SMU, both on soil Class B profiles and 12 km from the focus, recorded PGAs of 0.24 and 0.18g during this event. The GMPE equation gave a value of 0.25g, which was selected as a_{max} for this event, because the hypocentral distance to Avasinis was slightly smaller than 12 km. For the M_w6.0 event, the hypocentral distance from Avasinis was 14.5 km. PGAs at strong motion recording stations GMN (12-km distance) and SRC0 (19-km distance), both on soil Class B profiles, were 0.26 and 0.24g, respectively, for this event. The GMPE and ShakeMap estimated PGAs of 0.27 and 0.25, respectively, which are very consistent with the measured PGA. An a_{max} of 0.25g was selected for this event based on the average of the recordings and predictions.

For the M_w6.4 main event, the hypocentral distance from Avasinis was 20 km. The only relevant strong motion recording station, TLM1, was located on a soil Class B profile at a hypocentral distance of 28 km and registered a PGA of 0.34g. The GMPE and ShakeMap estimated PGAs of 0.47 and 0.45, respectively, which are very consistent, but 35% higher than at the recording station because of the smaller source-to-site distance. An a_{max} of 0.46g (average of GMPE and ShakeMap values) was selected for this event because the actual hypocentral distance was 8 km closer than the recording station. Boulanger and Idriss (2014) also used ShakeMap to revise PGA values in their data set where necessary. The earthquake parameters are listed in Table 3 along with MSF values for each case, CSRs, and CSR/MSF values in the critical layers.

The CSR and DPT N'_{120} values for the Friuli case histories are plotted in Fig. 11 for comparison with the triggering curves developed previously by Cao et al. (2013). The data points for DPTs 1, 2, and 3 for the main shock (M_w6.4) all fall on or above the 70% probability curve. However, the data points for the smaller aftershocks (M_w6.0 and 5.3) at Site 1, where liquefaction was observed, typically plot on or above the 30% probability curve. No observations were made at the other sites for the aftershocks. Thus, these three data points correctly predict the occurrence of liquefaction surface features. Because these data points are some of the lowest of any in the overall data set, they could be particularly important in refining the shape of the triggering curve in the future.

For DPT 4, the CSR-N'_{120} data point also plots above the 85% probability of liquefaction curve; however, the site did not exhibit evidence of liquefaction. The critical zone of liquefaction is located within the zone from 1.5 to 4.0 m. A review of the soil profile in Fig. 7(b) indicates that this layer consists of interbedded silt and silty sandy gravel layers. Some grain-size distribution curves for the layers in this profile are shown in Fig. 3 based on samples from core holes adjacent to the DPT hole. Fines contents for the silty sandy gravel layers in the zone of liquefaction are typically high (18% and 26%). Other researchers have observed false-positive predictions (layers predicted to liquefy but without manifestation of liquefaction; e.g., sand boils, settlement, lateral spreading) in layers consisting of highly interbedded silt and sand layers at sites

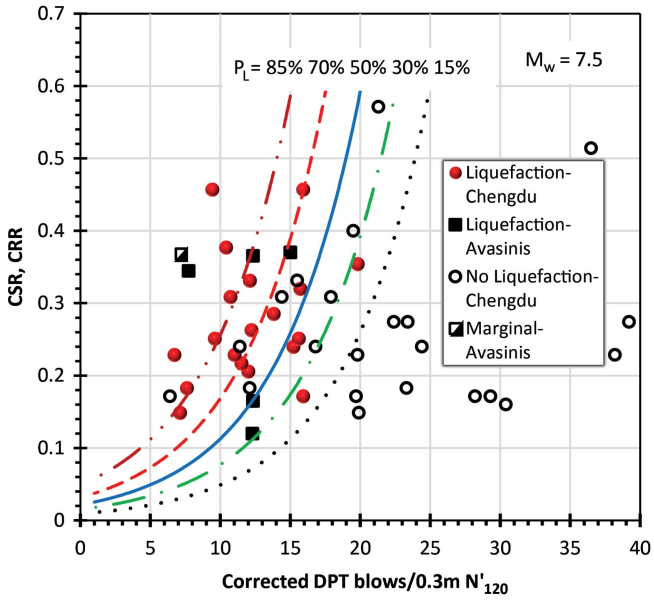

Fig. 11. Probabilistic liquefaction-triggering curves for gravelly soils based on DPT penetration resistance after scaling to a M_w7.5 earthquake. Liquefaction and no-liquefaction data points are from Chengdu, China, and Avasinis, Italy. (Adapted from Cao et al. 2013, © ASCE.)

in Turkey (Youd et al. 2009) and Christchurch, New Zealand (Cubrinovski et al. 2017).

In studies reported in two keynote papers and a journal article, Cubrinovski et al. (2017, 2018, 2019) studied 15 sites where liquefaction was predicted and surface effects of liquefaction were observed, along with 17 sites where liquefaction was predicted but no surface effects were observed. They found that there was no difference in the average CPT penetration resistance in the critical liquefaction layers for sites that did or did not manifest liquefaction during the Christchurch earthquake sequence from 2010 to 2011. They attributed the difference to the "system response" of the profile. The 15 sites that produced surface effects of liquefaction had thicker, more uniform, and vertically continuous layers of liquefiable soil, without surface layers of nonliquefiable soil. Liquefaction produced large volumes of water in the thick critical layer, which was supplemented by upward flow from the liquefied soil below it, so that system response combined to promote the eruption of sand ejecta at the ground surface.

In contrast, the 17 sites that did not produce surface effects of liquefaction, despite being predicted to liquefy, were composed of "highly stratified deposits consisting of interbedded liquefiable and nonliquefiable layers," thin and vertically discontinuous liquefiable layers, and liquefiable layers consisting of silty sands and silts. These profiles also contained separate liquefiable layers 7–10 m below the ground surface, much below the critical layer. Effective stress-based numerical analyses conducted by Cubrinovski et al. (2017) indicate that liquefaction of the deeper layers reduced acceleration levels in the critical zone, reducing the potential for pore pressure generation. Silty surface layers also tended to be partially saturated, which also increased liquefaction resistance. Ejecta from the deeper liquefied layer was unlikely to erupt to the surface because of the interbedded layer above it. Even though liquefaction may still have occurred in the thin discontinuous critical layers, the upward flow volume would have been much smaller and would have been impeded by the interbedded low-permeability layers

preventing the eruption of sand boils. Thus, system response combined to inhibit surface manifestation of liquefaction.

The soil profile at Site 4 in Avasinis, Italy, is very similar to the sites in Christchurch, New Zealand, that were predicted to liquefy but showed no surface effects of liquefaction, except that the liquefiable layers in Avasinis contain gravel. It is therefore reasonable to conclude that these gravelly layers may have liquefied but did not manifest surface evidence of liquefaction because of the system response of the profile as explained by Cubrinovski et al. (2017, 2018, 2019). Because the simplified approach used in this study does not presently consider the effects of system response, we believe that the data point for Site 4 cannot be conclusively placed in either the "liquefaction" or "no liquefaction" category. Because of this uncertainty, we have classified the CSR-N'_{120} data point for Site 4 as "marginal" on the subsequent triggering plots (Figs. 11 and 13).

Comparison with SPT-Based Liquefaction-Triggering Curves

The $(N_1)_{60}$-versus-depth profile from the SPT testing near DPT 1 and DPT 2 was shown in Figs. 4(b) and 5(b). At Sites 1 and 2, the average fines contents are 13 and 10, respectively (Sirovich 1996a). CSR-versus-$(N_1)_{60,cs}$ values are plotted in Fig. 12 for the three Friuli earthquakes at Site 1 and for the main shock at Site 2, relative to the triggering curves proposed by (a) Idriss and Boulanger (2008) and (b) Youd et al. (2001). CSR and $(N_1)_{60,cs}$ values differ for the two plots because of a variety of differences in the two procedures, including the MSFs. The data points for the main shock (M_w6.4) clearly plot above the triggering curve, which agrees with the observed liquefaction features. For the aftershocks, the data points for the M_w6.0 event fall just above the triggering curve, whereas the data points for the M_w5.3 event fall on or slightly below the curve, even though liquefaction features were observed. Results similar to those for Idriss and Boulanger (2008) were also obtained with the Cetin et al. (2004) approach but are not shown because of space constraints.

Therefore, the SPT-based procedures were generally successful in predicting the observed liquefaction for the loose gravelly sands involved. This result is consistent with findings by others in loose gravelly sands with limited gravel content (Rhinehart et al. 2016; Yan and Lum 2003; Andrus 1994). Of course, SPT-based liquefaction assessment in gravelly soil becomes more problematic when blow counts are high, but it is uncertain whether this is a result of higher density or interference from gravel-sized particles.

Finally, it should be noted that if the SPT $(N_1)_{60}$ at Site 4 were obtained from the correlation with the DPT N'_{120}, liquefaction would also be predicted for the critical layer despite the lack of surface manifestations of liquefaction. Thus, the SPT would likely produce a false positive for this site, along with the DPT.

Comparison with V_S-based Liquefaction-Triggering Curves

Liquefaction-triggering curves based on overburden stress corrected shear wave velocity (V_{S1}) have been proposed by several researchers (e.g., Andrus and Stokoe 2000; Kayen et al. 2013) based on sand liquefaction data. The triggering curve for the Kayen et al. (2013) approach was set equal to the 15% probability of liquefaction curve as recommended by the authors. Critical liquefaction zones for each DPT site were selected using the measured V_{S1} profiles as shown in Figs. 4(c)–7(c). They are generally similar to those for the DPT blow counts, but not identical. This could result from the MASW inversion process. At DPT 1, the average velocity of 200 m/s in the top 12 m of the profile obtained from the cross-hole testing is used. However, at the other sites, the V_{S1} is based on the joint inversion of the H/V and MASW dispersion curves.

The CSR values for the four Avasinis case histories are plotted versus the measured V_{S1} in Fig. 13 for (a) the Andrus and Stokoe (2000) triggering curve and (b) the Kayen et al. (2013) triggering curve for a fines content of 13%. The procedures for computing the r_d and magnitude scaling factors are different for the two methods and led to somewhat different CSR values. For the Andrus and Stokoe (2000) curve, four of the five liquefaction data points plot below the liquefaction-triggering curve, indicating inaccurate prediction of the liquefaction potential. For the Kayen et al. (2013) method, where the triggering curve is shifted toward a higher V_{S1}, two points from the main shock are consistent with liquefaction, and the remaining three points are slightly below the boundary. Other investigators have reported similar inaccuracies in predicting

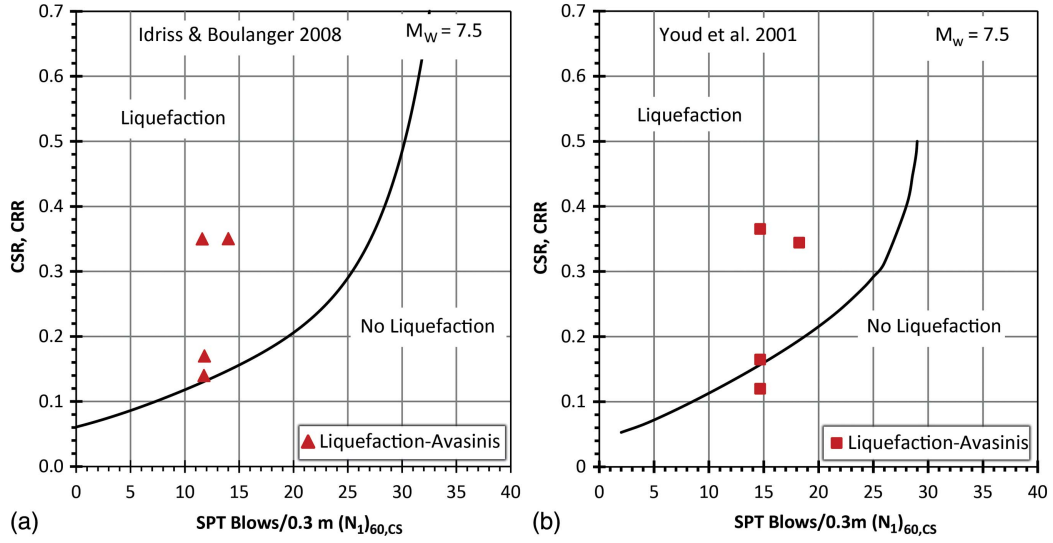

Fig. 12. Liquefaction-triggering curves for clean sand based on SPT $(N_1)_{60,cs}$ proposed by (a) Idriss and Boulanger (2008); and (b) Youd et al. (2001) for a M_w7.5 earthquake relative to liquefaction case histories involving gravelly sand at Sites 1 and 2.

J. Geotech. Geoenviron. Eng., 2020, 146(6): 04020038

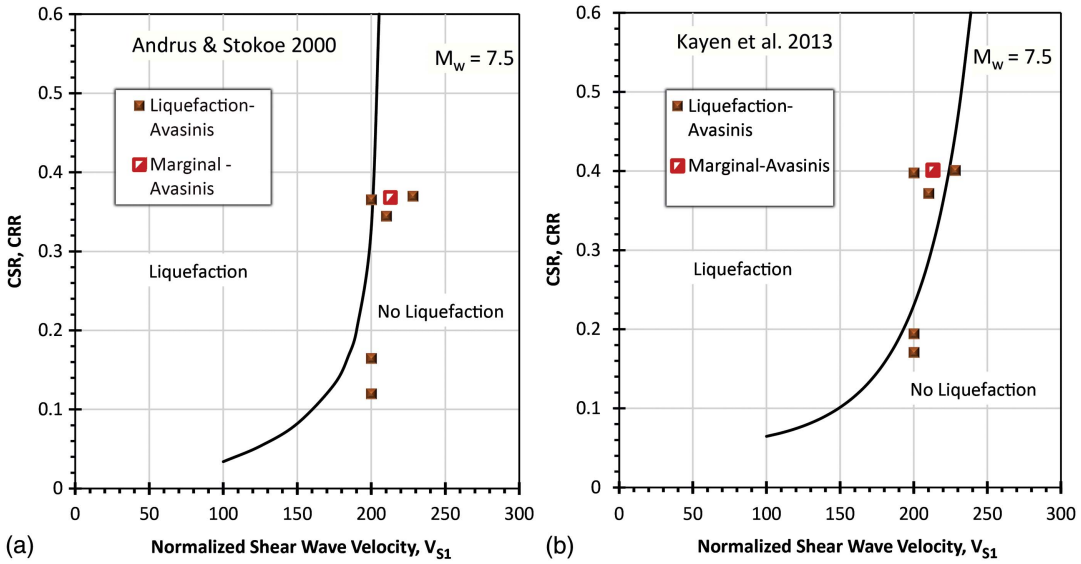

Fig. 13. Liquefaction-triggering curves for sand with 13% fines based on normalized shear wave velocity (V_{S1}) proposed by (a) Andrus and Stokoe (2000); and (b) Kayen et al. (2013) for a M_w7.5 earthquake relative to liquefaction case histories involving gravelly sand at Avasinis sites.

liquefaction of gravelly soils using shear wave velocity (Cao et al. 2013; Rollins et al. 1998; Chang et al. 2016) by use of curves developed for sands. Therefore, some adjustment of the V_{S1} triggering curves may be desirable for gravelly soil profiles. The CSR-V_{S1} data point for Site 4, which did not exhibit liquefaction features, plots within the cluster of data points for Sites 1, 2, and 3 that did have liquefaction features. Thus, V_{S1} was also unable to distinguish observed behavior at this site.

Conclusions

Based on investigations conducted using the Chinese Dynamic Cone Penetrometer (DPT) test at Avasinis, Italy, the following conclusions have been reached:

1. The Chinese Dynamic Cone Penetrometer could generally be driven through sandy gravel alluvium profiles with 20%–40% gravel content using only the conventional SPT hammer energy despite the larger particle sizes.
2. Typical hammer energy correction factors (Seed et al. 1985) provide a reasonable means for adjusting the blow count from the SPT hammer to give blow counts that would be obtained with the conventional Chinese DPT hammer energy for N'_{120} values less than 20. However, some adjustments for greater depths, N'_{120} values, or gravel percentages may be necessary when additional information is collected. Use of the heavier hammer for liquefaction assessment avoids uncertainty associated with scatter in the energy correction, but the lighter hammer can provide greater resolution for loose layers.
3. Liquefaction-triggering correlations based on the DPT N'_{120} value correctly identified all three sites (Sites 1–3) where liquefaction features were observed in loose to medium dense, thickly bedded gravelly sand profiles with 20%–40% gravel and fines content less than 15%.
4. Liquefaction-triggering correlations based on the DPT N'_{120} value incorrectly predicted liquefaction in a soil profile with highly interbedded silt and silty sandy gravel layers (Site 4) that produced no surface evidence of liquefaction despite low blow counts. This false positive is consistent with false positives from CPT testing in highly interbedded silt and sand layers in Christchurch, New Zealand, and is likely a result of the system response of the profile, which inhibited eruption of ejecta as explained by Cubrinovski et al. (2017, 2018, 2019). Prediction of liquefaction behavior in similar interbedded profiles is likely to be problematic for all penetration resistance correlations, and they should be used with judgment.
5. Triggering curves based on the SPT $(N_1)_{60,cs}$ values were generally successful in predicting liquefaction for two loose to medium dense, gravelly sand sites (Sites 1 and 2), with 20%–40% gravel and less than 15% fines, although one point from an aftershock was on or below the boundary, depending on the triggering curve. However, $(N_1)_{60}$ values obtained from correlation with the DPT N'_{120} values suggest that the SPT likely would have also produced a false positive for the interbedded profile at Site 4.
6. The Andrus and Stokoe (2000) triggering curve based on the normalized shear wave velocity (V_{S1}) predicted no liquefaction for four of five cases where liquefaction features were observed in the field. In contrast, the Kayen et al. (2013) V_{S1}-based triggering curve appeared to be more consistent with field performance for the main shock but produced some false negatives for the aftershocks. This is consistent with previous research (Rollins et al. 1998; Cao et al. 2013; Chang 2016) in which V_{S1} correlations produced false negatives in gravelly sands. Therefore, liquefaction-triggering curves for gravelly soil may need to be adjusted to somewhat higher velocities. The CSR-V_{S1} data point for Site 4, which did not exhibit liquefaction features, plots within the cluster of data points for Sites 1, 2, and 3 that did have liquefaction features. Thus, V_{S1} was also unable to distinguish observed behavior at this site.

Acknowledgments

Funding for this study was provided by grant G16AP00108 from the US Geological Survey Earthquake Hazard Reduction Program and grant CMMI-1663288 from the National Science Foundation. This funding is gratefully acknowledged; however, the opinions, conclusions, and recommendations in this paper do not necessarily represent those of the sponsors. We are grateful to Gerhart-Cole,

Inc. (Midvale, Utah), for donating the PDA equipment used in this study. Funding for the MASW and H/V testing was provided by Istituto Nazionale di Geofisica e Vulcanologia. A special thanks to Livio Sirovich for kindly sharing his valuable dataset and his deep knowledge on the Friuli earthquake. Thanks also to the Avasinis Municipality and geologist Davide Serravalli for sharing the seismic microzonation studies; to geologist Maria Rosaria Manuel for the proper performance of the DPT tests; and to Prof. Marco Stefani for an overview on the geological context.

Supplemental Data

Figs. S1–S3 and Table S1 are available online in the ASCE Library (www.ascelibrary.org).

References

AASHTO. 1995. *Standard specification for classification of soils and soil-aggregate mixtures for highway construction purposes*. AASHTO M 145. Washington, DC: AASHTO.

Andrus, R. D. 1994. "In situ characterization of gravelly soils that liquefied in the 1983 Borah Peak earthquake." Ph.D. dissertation, Univ. of Texas at Austin, Dept. of Civil Engineering.

Andrus, R. D., and K. H. Stokoe II. 2000. "Liquefaction resistance of soils from shear-wave velocity." *J. Geotech. Eng.* 126 (11): 1015–1025. https://doi.org/10.1061/(ASCE)1090-0241(2000)126:11(1015).

Bindi, D., F. Pacor, L. Luzi, R. Puglia, M. Massa, G. Ameri, and R. Paolucci. 2011. "Ground motion prediction equations derived from the Italian strong motion database." *Bull. Earthquake Eng.* 9 (6): 1899–1920. https://doi.org/10.1007/s10518-011-9313-z.

Bonnefoy-Claudet, S., C. Cornou, P. Y. Bard, F. Cotton, P. Moczo, J. Kristek, and D. Fäh. 2006. "H/V ratio: A tool for site effects evaluation. Results from 1-D noise simulations." *Geophys. J. Int.* 167 (2): 827–837. https://doi.org/10.1111/j.1365-246X.2006.03154.x.

Boulanger, R. W., and I. M. Idriss. 2014. *CPT and SPT based liquefaction triggering procedures*, 134. Rep. No. UCD/CGM-14/01. Davis, CA: Center for Geotechnical Modeling, Dept. of Civil and Environmental Engineering, Univ. of Calif, Davis.

BSI (British Standard Institution). 2015. *Code of practice for ground investigations*. BS 5930. London: BSI.

Cao, Z., K. M. Rollins, X. M. Yuan, T. L. Youd, M. Talbot, J. Roy, and S. Amoroso. 2019. "Applicability and reliability of CYY formula based on Chinese dynamic penetration test for liquefaction evaluation of gravelly soils." *Chin. J. Geotech. Eng.* 41 (9): 1628–1634. https://doi.org/10.11779/CJGE201601018.

Cao, Z., T. Youd, and X. Yuan. 2013. "Chinese dynamic penetration test for liquefaction evaluation in gravelly soils." *J. Geotech. Eng.* 139 (8): 1320–1333. https://doi.org/10.1061/(ASCE)GT.1943-5606.0000857.

Cao, Z., T. L. Youd, and X. Yuan. 2011. "Gravelly soils that liquefied during 2008 Wenchuan, China Earthquake, Ms=8.0." *Soil Dyn. Earthquake Eng.* 31 (8): 1132–1143. https://doi.org/10.1016/j.soildyn.2011.04.001.

Cao, Z., X. Yuan, T. L. Youd, and K. M. Rollins. 2012. "Chinese dynamic penetration tests (DPT) at liquefaction sites following 2008 Wenchuan Earthquake." In *Proc., 4th Int. Conf. on Geotechnical and Geophysical Site Characterization*, 1499–1504. London: Taylor & Francis.

Cetin, K. O., R. B. Seed, A. Der Kiureghian, K. Tokimatsu, L. F. Harder, R. E. Kayen, and R. E. Moss. 2004. "Standard penetration test-based probabilistic and deterministic assessment of seismic soil liquefaction potential." *J. Geotech. Geoenviron. Eng.* 130 (12): 1314–1340. https://doi.org/10.1061/(ASCE)1090-0241(2004)130:12(1314).

Chang, W. J. 2016. "Evaluation of liquefaction resistance for gravelly sands using gravel content-corrected shear-wave velocity." *J. Geotech. Geoenviron. Eng.* 142 (5): 04016002. https://doi.org/10.1061/(ASCE)GT.1943-5606.0001427.

Chinese Design Code. 2001. *Design code for building foundation of Chengdu region*. [In Chinese.] DB51/T5026-2001. Sichuan Province, Chengdu, China: Administration of Quality and Technology.

Coulter, H. W., and R. R. Migliaccio. 1966. *Effect of the earthquake of March 22, 1964 at Valdez. Alaska*. Reston, VA: U.S. Geological Survey.

Cox, B. R., and D. P. Teague. 2016. "Layering ratios: A systematic approach to the inversion of surface wave data in the absence of apriori information." *Geophys. J. Int.* 207 (1): 422–438. https://doi.org/10.1093/gji/ggw282.

Cubrinovski, M., N. Ntritsos, R. Dhakal, and A. Rhodes. 2019. "Key aspects in the engineering assessment of soil liquefaction." In *Proc., 7th Int. Conf. on Earthquake Geotechnical Engineering*, 189–208. Abingdon, UK: Taylor & Francis Group.

Cubrinovski, M., A. Rhodes, N. Ntritsos, and S. Van Ballegooy. 2017. "System response of liquefiable deposits." In *Proc., Performance Based Design III*, 18. London: International Society for Soil Mechanics and Geotechnical Engineering.

Cubrinovski, M., A. Rhodes, N. Ntritsos, and S. Van Ballegooy. 2018. "System response of liquefiable deposits." *J. Soil Dyn. Earthquake Eng.* 124 (Sep): 212–229. https://doi.org/10.1016/j.soildyn.2018.05.013.

De Jong, J. T., M. Ghafghazi, A. P. Sturm, D. W. Wilson, J. den Dulk, R. J. Armstrong, A. Perez, and C. A. Davis. 2017. "Instrumented Becker penetration test. I: Equipment, operation, and performance." *J. Geotech. Geoenviron. Eng.* 143 (9): 04017062. https://doi.org/10.1061/(ASCE)GT.1943-5606.0001717.

Engemoen, W. 2007. *Evaluation of in-situ methods for liquefaction investigation of dams*. Rep. No. DSO-07-09. Washington, DC: Bureau of Reclamation.

Fäh, D., F. Kind, and D. Giardini. 2003. "Inversion of local S-wave velocity structures from average H/V ratios, and their use for the estimation of site-effects." *J. Seismolog.* 7 (4): 449–467. https://doi.org/10.1023/B:JOSE.0000005712.86058.42.

Fontana, A., P. Mozzi, and A. Bondesan. 2008. "Alluvial megafans in the Veneto-Friuli Plain: Evidence of aggrading and erosive phases during late Pleistocene and Holocene." *Quat. Int.* 189 (1): 71–90. https://doi.org/10.1016/j.quaint.2007.08.044.

Foti, S., et al. 2017. "Guidelines for the good practice of surface wave analysis: A product of the Interpacific project." *Bull. Earthquake Eng.* 16 (6): 2367–2420. https://doi.org/10.1007/s10518-017-0206-7.

García-Jerez, A., J. Piña-Flores, F. J. Sánchez-Sesma, F. Luzón, and M. Perton. 2016. "A computer code for forward calculation and inversion of the H/V spectral ratio under the diffuse field assumption." *Comput. Geosci.* 97 (Dec): 67–78. https://doi.org/10.1016/j.cageo.2016.06.016.

Green, R. A., M. Cubrinovski, B. Cox, C. Wood, L. Wotherspoon, B. Bradley, and B. Maurer. 2014. "Select liquefaction case histories from the 2010-2011 Canterbury earthquake sequence." *Earthquake Spectra* 30 (1): 131–153. https://doi.org/10.1193/030713EQS066M.

Harder, L. F. 1997. *Application of the Becker penetration test for evaluating the liquefaction potential of gravelly soils*. Technical Rep. NCEER-97-0022. Buffalo, NY: National Center for Earthquake Engineering Research, Univ. at Buffalo.

Idriss, I., and R. W. Boulanger. 2008. *Soil liquefaction during earthquakes*. Oakland, CA: Earthquake Engineering Research Institute.

Ishihara, K. 1985. "Stability of natural deposits during earthquakes." In *Proc., 11th Int. Conf. on Soil Mechanical and Foundation Engineering*, 321–376. Rotterdam, Netherlands: A.A. Balkema.

ISO. 2018. *Geotechnical investigation and testing—Identification and classification of soil—Part 1: Identification and description*. ISO 14688-1:2017. Geneva: ISO.

ISSMFE Technical Committee on Penetration Testing. 1988. "Standard penetration test (SPT): International reference test procedure." In *Proc. 1st Int. Symp. on Penetration Testing, ISOPT-1*, 3–26. Rotterdam, Netherlands: A.A. Balkema.

Kayen, R., R. E. S. Moss, E. M. Thompson, R. B. Seed, K. O. Cetin, A. Der Kiureghian, Y. Tanaka, and K. Tokimatsu. 2013. "Shear-wave velocity-based probabilistic and deterministic assessment of seismic soil liquefaction potential." *J. Geotech. Geoenviron. Eng.* 139 (3): 407–419. https://doi.org/10.1061/(ASCE)GT.1943-5606.0000743.

Kayen, R. E., J. K. Mitchell, R. B. Seed, A. Lodge, S. Nishio, and R. Coutinho. 1992. *Evaluation of SPT-, CPT-, and shear wave-based methods for liquefaction potential assessment using Loma Prieta data*.

Technical Rep. NCEER-97-0022. Buffalo, NY: National Center for Earthquake Engineering Research, Univ. at Buffalo.
Kokusho, T., Y. Tanaka, K. Kudo, and T. Kawai. 1995. "Liquefaction case study of volcanic gravel layer during 1993 Hokkaido-Nansei-Oki earthquake." In *Proc., 3rd Int. Conf. on Recent Advances in Geotechnical Earthquake Engineering and Soil Dynamics*, 235–242. Rolla, MO: Missouri Univ. of Science and Technology.
Kokusho, T., and Y. Yoshida. 1997. "SPT N-value and S-wave velocity for gravelly soils with different grain size distribution." *Soils Found.* 37 (4): 105–113. https://doi.org/10.3208/sandf.37.4_105.
Kovacs, W. D., L. A. Salomone, and F. Y. Yokel. 1983. *Comparison of energy measurements in the standard penetration test using the cathead and rope method, Phases I and II, Final Report*. NUREGI 37CR-3545. Washington, DC: The Division.
Kulhawy, F. H., and P. W. Mayne. 1990. *Manual on estimating soil properties for foundation design*. Palo Alto, CA: Electric Power Research Institute.
Liao, S., and R. V. Whitman. 1986. "Overburden correction factors for SPT in sand." *J. Geotech. Eng.* 112 (3): 373–377. https://doi.org/10.1061/(ASCE)0733-9410(1986)112:3(373).
Lin, P.-S., and C.-W. Chang. 2002. "Damage investigation and liquefaction potential analysis of gravelly soil." *J. Chin. Inst. Eng.* 25 (5): 543–554.
Lopez, S., X. Vera-Grunauer, K. Rollins, and G. Salvatierra. 2018. "Gravelly soil liquefaction after the 2016 Ecuador Earthquake." In *Proc., Conf. on Geotechnical Earthquake Engineering and Soil Dynamics V*, 273–285. Reston, VA: ASCE.
Luzi, L., R. Puglia, E. Russo, and ORFEUS WG5. 2016. "Engineering strong motion database, version 1.0." In *Observatories & research facilities for European seismology*. Rome, Italy: Istituto Nazionale di Geofisica e Vulcanologia.
Maurenbrecher P. M., A. Den Outer, and H. J. Luger. 1995. "Review of geotechnical investigations resulting from the Roermond April 13, 1992 earthquake." In *Proc., 3rd Int. Conf. on Recent Advances in Geotechnical Earthquake Engineering and Soil Dynamics*, 645–652. Rolla, MO: Missouri Univ. of Science and Technology.
Menq, F. Y. 2003. "Dynamic properties of sandy and gravelly soils." Ph.D. dissertation, Dept. of Civil, Architectural and Environmental Engineering, Univ. of Texas.
Nakamura, Y. 1989. "A method for dynamic characteristics estimation of subsurface using microtremor on the ground surface." *Railway Tech. Res. Inst. Quart. Rep.* 30 (1): 25–33.
Nikolaou, S., D. Zekkos, D. Assimaki, and R. Gilsanz. 2014. "GEER/EERI/ATC earthquake reconnaissance January 26th/February 2nd 2014 Cephalonia, Greece Events, Version 1." Accessed February 28, 2020. http://www.geerassociation.org/administrator/components/com_geer_reports/geerfiles/ECUADOR_Report_GEER-049-v1b.pdf.
Park, C. B., R. D. Miller, and J. Xia. 1999. "Multichannel analysis of surface waves." *Geophysics* 64 (3): 800–808. https://doi.org/10.1190/1.1444590.
Piña-Flores, J., M. Perton, A. García-Jerez, E. Carmona, F. Luzón, J. Molina-Villegas, and F. Sánchez-Sesma. 2016. "The inversion of spectral ratio H/V in a layered system using the diffuse field assumption (DFA)." *Geophys. J. Int.* 208 (1): 577–588. https://doi.org/10.1093/gji/ggw416.
Rhinehart, R., A. Brusak, and N. Potter. 2016. *Liquefaction triggering assessment of gravelly soils: State-of-the-art review*. Rep. No. ST-2016-0712-01. Washington, DC: US Bureau of Reclamation.
Robertson, P. K., D. J. Woeller, and W. D. Finn. 1992. "Seismic cone penetration test for evaluating liquefaction potential under cyclic loading." *Can. Geotech. J.* 29 (4): 686–695. https://doi.org/10.1139/t92-075.
Rollins, K. M., N. B. Diehl, and T. J. Weaver. 1998. "Implications of V_s-BPT $(N_1)_{60}$ correlations for liquefaction assessment in gravels." In *Proc., Geotechnical Earthquake Engineering and Soil Dynamics, Geotechnical Special Pub. No. 75*, 506–517. Reston, VA: ASCE.
Sánchez-Sesma, F. J., M. Rodríguez, U. Iturrarán-Viveros, F. Luzón, M. Campillo, L. Margerin, A. García-Jerez, M. Suarez, M. A. Santoyo, and A. Rodríguez-Castellanos. 2011. "A theory for microtremor H/V spectral ratio: Application for a layered medium." *Geophys. J. Int.* 186 (1): 221–225. https://doi.org/10.1111/j.1365-246X.2011.05064.x.
Seed, H. B., K. Tokimatsu, L. F. Harder, and R. M. Chung. 1985. "Influence of SPT procedures in soil liquefaction resistance evaluations." *J. Geotech. Eng.* 111 (12): 1425–1445. https://doi.org/10.1061/(ASCE)0733-9410(1985)111:12(1425).
Serravalli D. 2016. "Seismic Microzonation study of I level for the Trasaghis municipality." [In Italian.] Accessed February 29, 2020. http://www.comune.trasaghis.ud.it/fileadmin/user_trasaghis/Ufficio_Tecnico/PRGC/Studio_microzonazione_sismica/MS/RELAZIONE_MS_TRASAGHIS.compressed.pdf.
Sirovich, L. 1996a. "In-situ testing of repeatedly liquefied gravels and liquefied overconsolidated sands." *Soils Found.* 36 (4): 35–44. https://doi.org/10.3208/sandf.36.4_35.
Sirovich, L. 1996b. "Repetitive liquefaction at gravelly site and liquefaction in overconsolidated sands." *Soils Found.* 36 (4): 23–34. https://doi.org/10.3208/sandf.36.4_23.
Stokoe, K. H. Jr. 2015. "47th Terzaghi lecture seismic measurements and geotechnical engineering." Accessed February 29, 2020. https://www.youtube.com/watch?v=jQMD1tC2KUA.
Sy, A. 1997. "Twentieth Canadian geotechnical colloquium: Recent developments in the Becker penetration test: 1986-1996." *Can. Geotech. J.* 34 (6): 952–973. https://doi.org/10.1139/t97-066.
Sykora, D. W. 1987. *Creation of a data base of seismic shear wave velocities for correlation analysis*. Vicksburg, MI: US Army Engineer Waterways Experiment Station.
Talbot, M. H. 2018. "Dynamic cone penetration tests for liquefaction evaluation of gravelly soils." Ph.D. dissertation, Civil and Environmental Engineering Dept., Brigham Young Univ.
Tokimatsu, K. 1997. "Geotechnical site characterization using surface waves." In *Proc., Earthquake Geotechnical Engineering*, 1333–1368. Rotterdam, Netherlands: A.A. Balkema.
Tokimatsu, K., and Y. Yoshimi. 1983. "Empirical correlation of soil liquefaction based on SPT N-value and fines content." *Soils Found.* 23 (4): 56–74. https://doi.org/10.3208/sandf1972.23.4_56.
Wang, W. S. 1984. "Earthquake damages to earth dams and levees in relation to soil liquefaction and weakness in soft clays." In *Proc., 1st Int. Conf. on Case Histories in Geotechnical Engineering*, 511–521. Rolla, MO: Missouri Univ. of Science and Technology.
Worden, C. B., E. M. Thompson, M. Hearne, and D. J. Wald. 2020. "ShakeMap V4 manual: Technical guide, user's guide, and software guide, U. S. Geological Survey." Accessed February 28, 2020. http://usgs.github.io/shakemap/index.html.
Yan L., and K. Y. Lum. 2003. "Liquefaction assessment of gravelly soils for dam safety evaluation." In *Proc., 21st Congress Int. Commission on Large Dams*. Paris: International Commission on Large Dams.
Yegian, M. K., V. G. Ghahraman, and R. N. Harutiunyan. 1994. "Liquefaction and embankment failure case histories, 1988 Armenia earthquake." *J. Geotech. Eng.* 120 (3): 581–596. https://doi.org/10.1061/(ASCE)0733-9410(1994)120:3(581).
Youd, T. L., et al. 2001. "Liquefaction resistance of soils: Summary Report from the 1996 NCEER and 1998 NCEER/NSF Workshops on evaluation of liquefaction resistance of soils." *J. Geotech. Geoenviron. Eng.* 135 (1): 46–61. https://doi.org/10.1061/(ASCE)1090-0241(2001)127:10(817).
Youd, T. L., D. W. De Dean, J. D. Bray, R. Sancio, K. O. Cetin, and T. M. Gerber. 2009. "Zero-displacement lateral spreads, 1999 Kocaeli, Turkey, Earthquake." *J. Geotech. Geoenviron. Eng.* 135 (1): 46–61. https://doi.org/10.1061/(ASCE)1090-0241(2009)135:1(46).
Youd, T. L., E. L. Harp, D. K. Keefer, and R. C. Wilson. 1985. "The Borah Peak, Idaho earthquake of October 29, 1983—Liquefaction." *Earthquake Spectra* 2 (1): 71–89. https://doi.org/10.1193/1.1585303.
Zanferrari, A., D. Masetti, G. Monegato, and M. E. Poli. 2013. "Note Illustrative della Carta Geologica d'Italia alla scala 1:50.000 Foglio 049 Gemona del Friuli." [In Italian.] Accessed February 29, 2020. http://www.isprambiente.gov.it/Media/carg/note_illustrative/49_Gemona%20_del_Friuli.pdf.